Quantitative NMR spectroscopy of supramolecular complexes: Dynamic side pores in ClpP are important for product release

Remco Sprangers*†§, Anna Gribun*, Peter M. Hwang*, Walid A. Houry*¶, and Lewis E. Kay*†§¶

Departments of *Biochemistry, †Medical Genetics, and §Chemistry, University of Toronto, Toronto, ON, Canada M5S 1A8

Edited by Alfred G. Redfield, Brandeis University, Waltham, MA, and approved September 30, 2005 (received for review August 23, 2005)

The highly conserved, 300-kDa cylindrical protease ClpP is an important component of the cellular protein quality machinery. It consists of 14 subunits arranged into two heptameric rings that enclose a large chamber containing the protease active sites. ClpP associates with ClpX and ClpA ATPases that unfold and translocate substrates into the protease catalytic chamber through axial pores located at both ends of the ClpP cylinder. Although the pathway of substrate delivery is well established, the pathway of product release is unknown. Here, we use recently developed transverse relaxation optimized spectroscopy (TROSY) of methyl groups to show that the interface between the heptameric rings exchanges between two structurally distinct conformations. The conformational exchange process has been quantified by magnetization exchange and methyl TROSY relaxation dispersion experiments recorded between 0.5°C and 40°C, so that the thermodynamic properties for the transition could be obtained. Restriction of the observed motional freedom in ClpP through the introduction of a cysteine linkage results in a protease where substrate release becomes significantly slowed relative to the rate observed in the reduced enzyme, suggesting that the observed motions lead to the formation of transient side pores that may play an important role in product release.

methyl transverse relaxation optimized spectroscopy | protein dynamics | ClpP protease

ClpP (1) is a representative member of the family of cylindrical self-compartmentalizing proteases (2, 3) that include the bacterial protein HslV (4) as well as the archaeal and eukaryotic 20S proteasomes (5, 6). The proteolytic active sites of these proteases are located in an enclosed catalytic chamber separated from the cellular milieu. Proteins targeted for degradation are recognized by AAA^+ chaperones that unfold and translocate substrates in an ATP-dependent manner into the lumen of the protease. In the case of ClpP (Fig. 1 *a–c*), it is well established that ClpX and ClpA deliver substrates through axial pores into the protease catalytic chamber for subsequent degradation (Fig. 1*a*) (1, 7, 8). In contrast, the pathway of product release remains controversial. For ClpP (1, 9, 10) and for the proteasome (11), it has been proposed that the entrance pores might also function as product exit sites. However, this proposal is problematic, because it requires the chaperones, which can bind to both ends of the protease simultaneously, to interrupt translocation to allow product release (12).

Recently, it has been shown that the ClpP handle region that forms the main interface between two ClpP rings (Fig. 1*b*) can be deleted without disrupting the oligomeric state of the protein. Furthermore, the x-ray structure of an A153P mutation of *Streptococcus pneumoniae* ClpP (13) shows that the mutation causes two turns of helix E to become unstructured. Nevertheless, the mutant protein remains a double heptamer, which suggests a high plasticity for the handle region (Fig. 1*d*). Here, we used recently developed NMR methodology (14, 15) and isotope labeling schemes (16) involving the use of methyl group probes to establish that the handle region is indeed dynamic, with an equilibrium between two distinct conformational states. Despite the high molecular mass of the complex (>300 kDa) and the low temperature used for many of the studies (0.5°C), it is, nevertheless, possible to obtain quantitative measures of both the kinetics and the thermodynamics of the exchange process. Where possible, results from one type of NMR experiment have been corroborated with those from a second, establishing that the NMR approaches are robust, even in applications involving supramolecular structures. Biochemical assays that are complimentary to the NMR study suggest a possible role for the dynamics in product release from ClpP. The present investigation shows that current NMR techniques are now at a stage where insight into biological function in even very large systems can be obtained.

Materials and Methods

Protein Expression and Purification. A pET9a vector overexpressing untagged WT *Escherichia coli* ClpP was a gift from John Flanagan (Brookhaven National Laboratory, Upton, NY). ClpP A153C, ClpP S111A A153C, ClpP ΔN (with a deletion of the 21 N-terminal residues, including the 14-residue prosequence), and ClpP ΔN S111A A153C were cloned into pET3a vectors without the prosequence and purified as described in ref. 17. ClpP I149V and I151L mutants were cloned into a modified pET-15b vector, which introduces an N-terminal histidine tag followed by a tobacco etch virus protease-recognition sequence. Point mutations were introduced with the QuikChange system (Stratagene) according to the manufacturer's protocol. U-[^{15}N,^{2}H], Ile δ1-[^{13}C,^{1}H] ClpP mutant samples were obtained by protein overexpression of the corresponding gene in BL21(DE3) cells in 250 ml of 100% D_2O minimal medium, as described in ref. 18. Purification was achieved by using Ni affinity chromatography, cleavage of the histidine tag, and size-exclusion chromatography. NMR experiments were performed on samples with protein monomer concentrations of 0.3–0.5 mM in 100% D_2O containing 50 mM potassium phosphate buffer (pH 6.8, uncorrected), 0.1 mM EDTA, 1 mM DTT, and 0.03% NaN_3. GFP-SsrA degradation assays, *N*-succinyl-Leu-Tyr-7-amido-4-methylcoumarin (Suc-LY-AMC) (Sigma) cleavage assays, and CD experiments were carried out as described in ref. 13.

Denaturing, Nonreducing SDS/PAGE. Oxidized forms of the ClpP A153C mutants were readily obtained in the absence of reducing agent. The oxidized forms were reduced by incubating with 10 mM DTT for 1 h at 37°C. To visualize the disulfide-linked forms of the ClpP A153C mutants on nonreducing SDS/PAGE gels,

Conflict of interest statement: No conflicts declared.

This paper was submitted directly (Track II) to the PNAS office.

Abbreviations: TROSY, transverse relaxation optimized spectroscopy; Suc-LY-AMC, *N*-succinyl-Leu-Tyr-7-amido-4-methylcoumarin.

¶To whom correspondence may be addressed. E-mail: walid.houry@utoronto.ca or kay@pound.med.utoronto.ca.

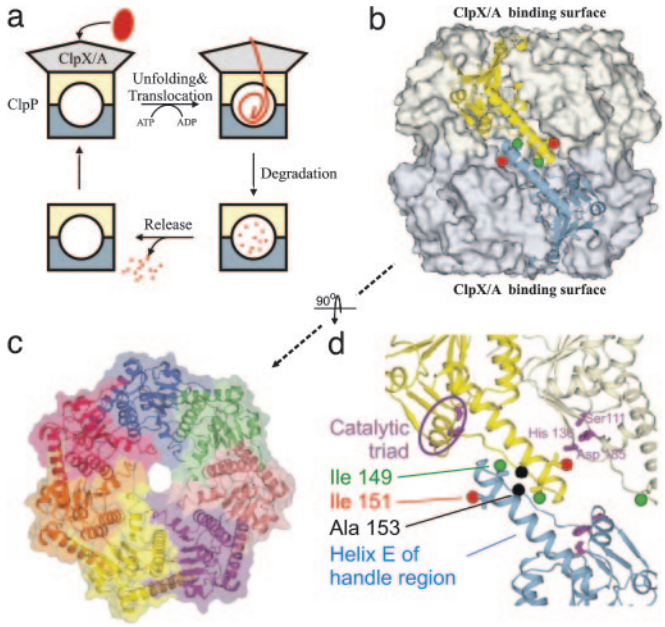

Fig. 1. ClpP structure and function. (*a*) Schematic diagram illustrating the mechanism of function of the ClpX/A–ClpP complex. ClpX/A unfolds and translocates substrate proteins into the ClpP proteolytic chamber for degradation in an ATP-dependent manner (8). ClpX/A molecules can bind ClpP from the top and bottom simultaneously. (*b* and *c*) *E. coli* ClpP side and top views. The axial pores are lined with the N-terminal residues of ClpP (13, 29) that are invisible in the *E. coli* x-ray structure (1). (*d*) Detailed view of the ClpP handle region. Residues of the catalytic triad are circled. The Cδ1 atoms of I149 and I151 are indicated by green and red spheres, respectively. The position of the A153C mutation is highlighted in black. Figures displaying molecular structures were prepared with PYMOL (www.pymol.org).

samples were incubated for 30 min with 55 mM iodoacetamide (Sigma) at 37°C, followed by additional heating at 95°C for 5 min.

Retention of Suc-LY-AMC by ClpP Cysteine Mutants. A ClpP cysteine mutant (20 μM) was incubated with 4.4 mM fluorogenic peptide, Suc-LY-AMC, in a total volume of 200 μl of buffer (25 mM Tris·HCl, pH 7.5/200 mM NaCl/10% glycerol) for 30 min at room temperature in the dark. The mixture was then applied on a calibrated Superdex 200 HR 10/30 column, and 1.0-ml fractions were collected over two column volumes. The fluorescence of the samples was measured on a Fluorolog 3-222 spectrofluorometer (Jobin Yvon, Longjumeau, France) using an excitation wavelength of 325 nm, and the emission scans were collected from 360 to 440 nm. Protein contents of the fractions were visualized on SDS/PAGE gels.

NMR Spectroscopy. NMR spectra were recorded with 600 and 800 MHz Varian Inova spectrometers equipped with cyro (600 MHz) or room-temperature (800 MHz) pulsed-field gradient triple resonance probes. All data were processed with the NMRPIPE/NMRDRAW suite of programs (19). Typical acquisition times for carbon chemical shift evolution were 20 ms, with the center of the carbon spectrum at 12.0 ppm. ^{1}H and ^{13}C chemical shift assignments are referenced against DSS (2,2-dimethyl-2-silapentane-5-sulfonate). Longitudinal magnetization transfer experiments were recorded as a series of 3D data sets with mixing times, t_{MIX}, between 0 and 60 ms. Briefly, magnetization is transferred from ^{1}H to ^{13}C, and the carbon chemical shift of the starting state is recorded (t_1). Subsequently, two-state longitudinal order is created that is allowed to exchange during a mixing time, followed by ^{13}C shift evolution (t_2) and transfer to ^{1}H for detection (t_3). The methyl transverse relaxation optimized spectroscopy (TROSY) principle (14) was exploited throughout the experiment. In this manner, correlations at (ω_{Ca}, ω_{Ca}, ω_{Ha}) and (ω_{Ca}, ω_{Cb}, ω_{Hb}) are obtained, corresponding to autopeaks and cross-peaks, respectively, where the two states are denoted by *a* or *b* and correspond to either S or F (see *Results and Discussion*). The data were fitted according to $I_{cross} = Ap_ap_b\exp(-\rho t_{MIX})[1 - \exp(-k_{ex}t_{MIX})]$ and $I_{auto} = B\exp(-\rho t_{MIX})[p_a^2 + p_ap_b\exp(-k_{ex}t_{MIX})]$, where $I_{cross/auto}$ is the intensity of the cross-/autopeak, $p_{a/b}$ is the population of state a/b, ρ is the longitudinal relaxation rate of the two-state order, H_zC_z (where X_Z is the Z magnetization of spin $X = \{H,C\}$), and k_{ex} is the exchange rate. Intensities were scaled according to the intensity of the corresponding autopeak at the shortest mixing time. The factors A and B take into account differential relaxation between the two states during the delays in the pulse sequence. Autorelaxation rates ρ were determined separately by using a 2D version of the exchange experiment where the first carbon evolution period was omitted. In the expressions for $I_{cross/auto}$ above, it is assumed that the autorelaxation rates for the two states are the same (i.e., $\rho_a = \rho_b$ for each residue, although they may differ for different residues). Indeed, measurements of ρ_a, ρ_b differ by <10% for either I149 or I151. In any event, the assumption of $\rho_a = \rho_b$ has little influence on the extracted rates or populations because ρ_a, $\rho_b \ll p_ak_{ex}$, p_bk_{ex}.

Methyl TROSY relaxation dispersion experiments (20) were recorded as a series of 2D data sets using constant-time relaxation periods of 15 ms (0.5°C), 10 ms (600 MHz, 35°C, 40°C), or 7 ms (800 MHz, 35°C, 40°C) and CPMG (Carr–Purcell–Meiboom–Gill) frequencies ranging from 66.7 to 1,000 Hz. $R_{2,eff}$, the effective transverse relaxation rate, is calculated according to $(-1/T)\ln(I/I_0)$, where I (or I_0) is the intensity of a correlation in the presence (or absence) of a constant-time relaxation interval of duration T, during which a variable number of ^{13}C 180° pulses are applied (20) and $\nu_{CPMG} = 1/(2\delta)$, where δ is the time between successive pulses. The dispersion data were fitted numerically as described in ref. 20. Chemical shift differences were initially estimated from spectra recorded at 0.5°C and then optimized based on the extracted exchange parameters from fits of the dispersion data. This optimization is accomplished in an iterative manner whereby the fitted exchange parameters are used, along with estimated shift differences, to obtain the true shift differences from the eigenvalues of the free precession evolution matrix. Errors in all exchange rates were estimated by using Monte Carlo methods based on the uncertainties in peak intensities.

Results and Discussion

NMR Resonance Assignment. The ClpP tetradecameric complex represents one of the largest systems studied quantitatively by using NMR methodologies. Unlike the case for NMR studies of the 900-kDa GroEL–GroES complex (21), ^{15}N-^{1}H correlation maps (22) for ClpP were of low quality, likely reflecting the large amount of dynamics in the oligomer (see below). By contrast, methyl TROSY (14) spectra of highly deuterated, Ileδ1-methyl protonated ClpP were of high quality. At least 12 of the expected 16 correlations are observed, even at temperatures as low as 0.5°C, where the rotational correlation time of the complex is estimated to be >400 ns (14). Ile probes are particularly useful in the present case, because the handle region contains two Ile residues (I149 and I151; Fig. 1 *b* and *d*) that can be used to report on the dynamics of this region.

Before a detailed NMR study, the chemical shifts of the isoleucines of interest must be assigned. The large size of ClpP precludes the use of traditional assignment strategies based on multidimensional experiments, and assignments were obtained by a mutational approach. For example, I149 and I151 were replaced by Val and Leu, respectively (Fig. 2*a*). Interestingly, in correlation spectra recorded at 0.5°C, δ1-methyls of both residues give rise to sets of two resonances (Fig. 2*a*), consistent with both isoleucines adopting a pair of distinct conformations.

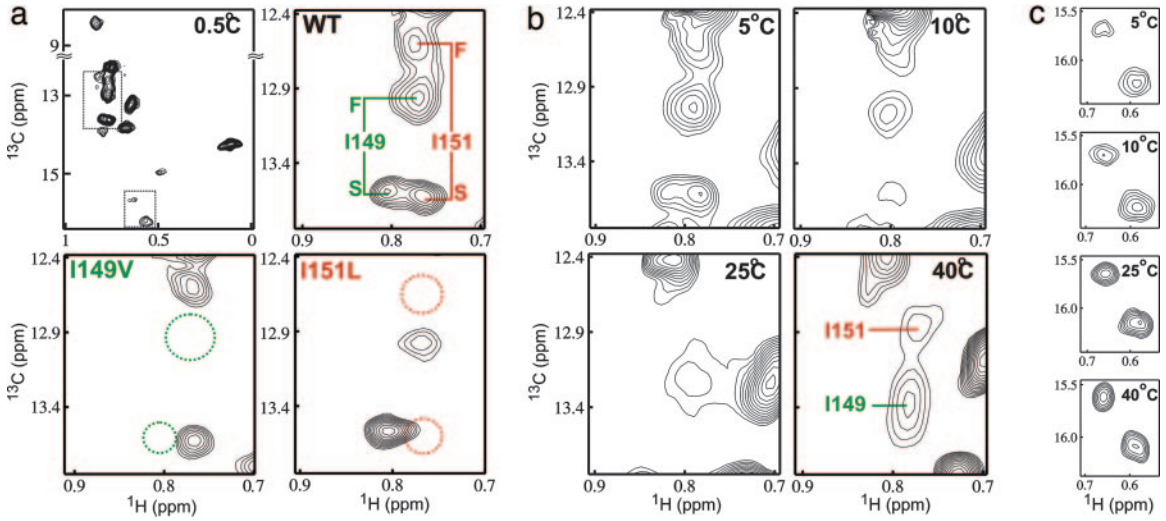

Fig. 2. Methyl TROSY heteronuclear multiple quantum correlation spectra of U-[^{15}N,^{2}H], Ile δ1-[^{13}C,^{1}H] ClpP protease (300 kDa). (*a*) Spectrum of WT ClpP at 0.5°C. The molecular tumbling time is predicted to be >400 ns (14). The upper boxed area is enlarged in *b*, and the lower boxed area is enlarged in *c*. Spectra of the ClpP I149V and I151L mutants are consistent with both isoleucines adopting at least two distinct conformations. The dotted circles indicate the positions of cross-peaks that are eliminated by either the I149V or I151L mutation. Note the different line widths for correlations derived from the two states, indicating a difference in internal mobility for state S (slowly relaxing) and F (fast relaxing). (*b*) Methyl TROSY spectra of WT ClpP showing increased exchange between states F and S as a function of temperature. (*c*) Representative correlations from nonexchanging Ile residues.

Notably, one correlation of the pair for both I149 and I151 is narrow and intense (Fig. 2*a*, WT), whereas a second is significantly broader. We have assigned the narrow cross-peaks as being derived from one state (S, for slow relaxation), and the broad cross-peaks are assigned to a second state (F, for fast relaxation). Increasing the temperature leads to a broadening of the resonances of both states, indicative of an increased rate of exchange between F and S. Between 15°C and 25°C, the resonances are broadened beyond detection, and they reappear as a single, averaged peak at temperatures >35°C (Fig. 2*b*). Because both isoleucines show the same temperature dependence, they likely undergo a common exchange process that may reflect a concerted motion of the handle regions at the interface between the two heptameric rings. The intensities of correlations from other residues increase throughout the complete temperature range (Fig. 2*c*), indicating that the observed exchange process is localized.

Kinetics and Thermodynamics of the F,S Exchange Process. To quantify the rates and energetics of the exchange process, we measured the time-dependent transfer of longitudinal two-spin order (23, 24) between sites from a series of 3D experiments (see *Materials and Methods*). Fitting the decay of the autopeaks and concomitant buildup of the exchange cross-peaks enables the extraction of both exchange rates and the populations of the

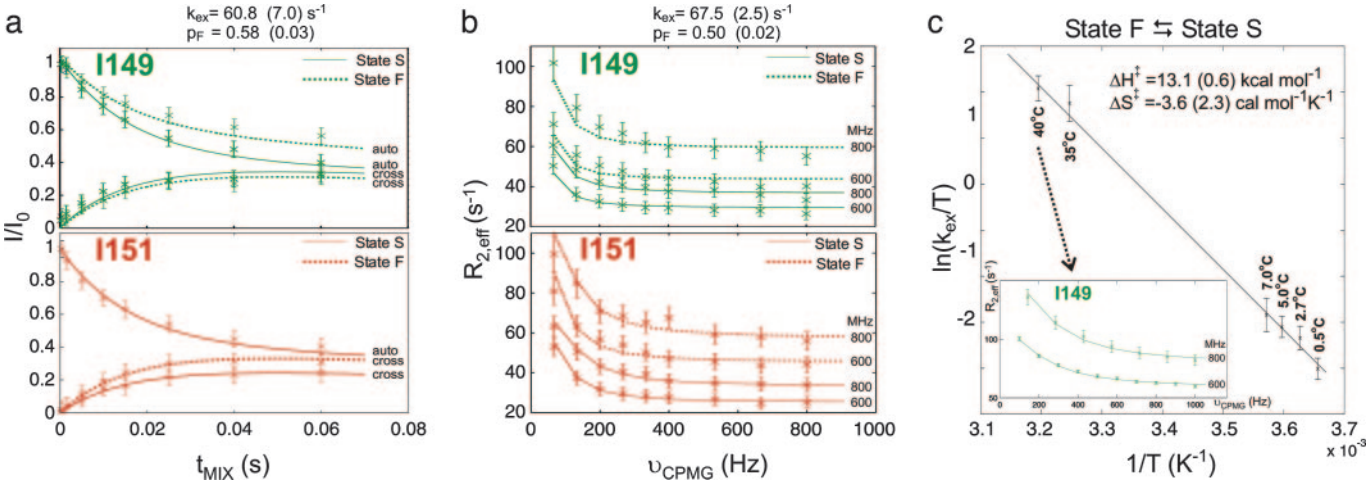

Fig. 3. Quantification of the F,S exchange process. (*a*) Longitudinal exchange spectroscopy recorded on WT ClpP at 0.5°C. The decay of autopeaks and buildup of cross-peaks is illustrated, where I/I_0 is the intensity of a given correlation normalized to the maximum intensity of the appropriate autopeak at the shortest time point used, uncorrected for any relaxation during the pulse scheme (see *Materials and Methods*). Experimental data points are indicated with "x," and the dotted and solid lines correspond to the best fits of the data for states F and S, respectively (all curves are fitted simultaneously). Because of spectral overlap, the autopeak derived from the I151 F state could not be quantified. (*b*) Methyl TROSY relaxation dispersion profiles recorded at 0.5°C. Contributions to relaxation rates from carbon chemical shift anisotropy as well as differences in ^{1}H chemical shifts between states result in differences in plateau values for the curves associated with a given state (F or S) at 600 and 800 MHz. (*c*) Determination of the activation energies that characterize the F,S exchange process. Note that $k_{F\rightarrow S} \approx k_{S\rightarrow F}$ so that the activation parameters are very similar for F→S and S→F. The relaxation dispersion profile of I149 recorded at 40°C is shown in *Inset*.

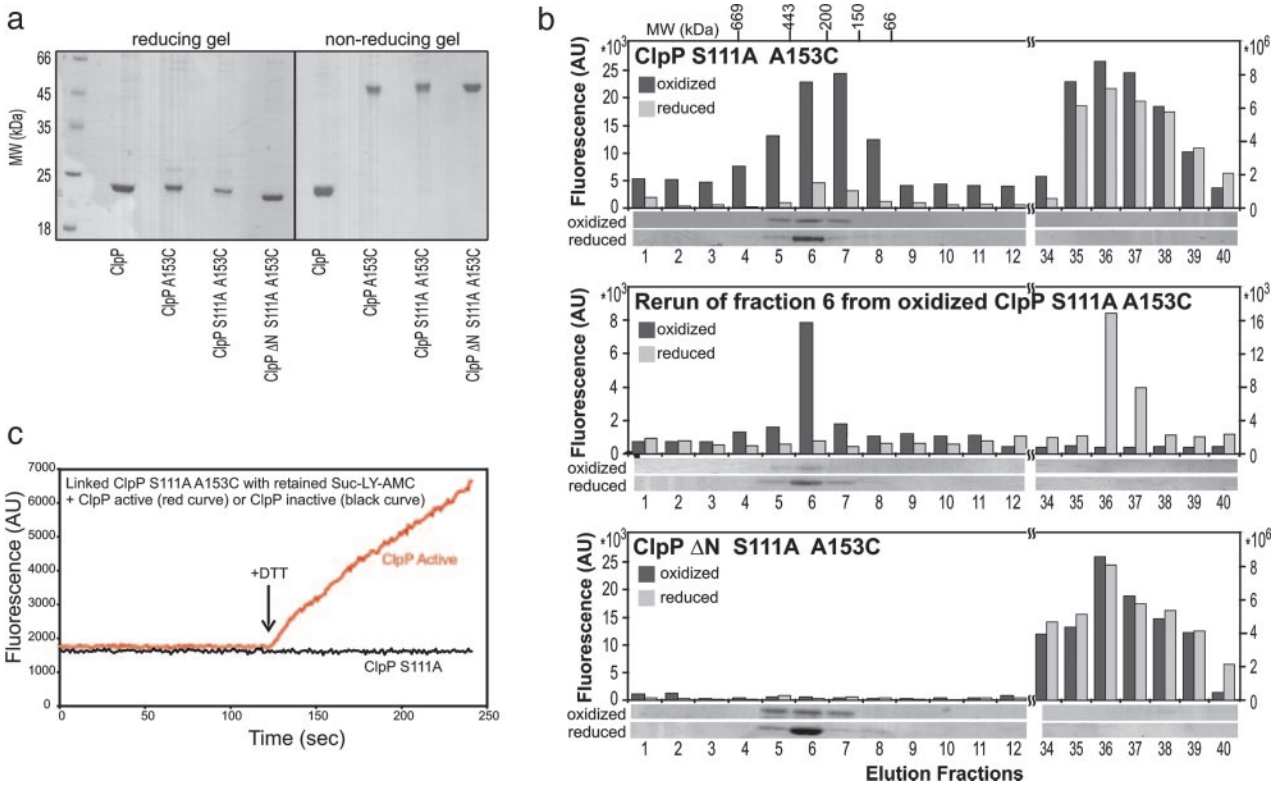

Fig. 4. The flexible handle regions affect product release. (*a*) SDS/PAGE analysis of ClpP WT and ClpP A153C mutants. Under reducing, denaturing conditions, all proteins migrate as monomers. Under nonreducing, denaturing conditions, the Cys mutants migrate as dimers, linked by disulfides at Cys-153. The position of the disulfide link and the molecular weight under nonreducing denaturing conditions has been verified by mass spectrometry (data not shown). (*b*) Size-exclusion chromatography profiles (using a calibrated Superdex 200 column) of ClpP incubated with Suc-LY-AMC fluorescent peptide. The fluorescence of each fraction (probing the presence/absence of peptide) was measured (bar graphs), and the protein content was visualized by SDS/PAGE analysis (below bar graphs). (*Top*) Under oxidizing conditions, the peptide is retained in the linked form of ClpP S111A A153C. Excess peptide in the incubation mixture that is not in the lumen of the protease elutes at 1.5× the column volume because the free peptide interacts weakly with the column. No peptide is retained under reducing conditions. (*Middle*) Fraction 6 from the experiment under oxidizing conditions in *Top* was rerun on the column. The peptide remains in the lumen of the protease under oxidizing conditions and is released under reducing conditions. (*Bottom*) ClpP ΔN S111A A153C does not retain the peptide, likely reflecting that deletion increases the size of the axial pores. (*c*) Inactive, oxidized ClpP (S111A A153C) was incubated with the fluorescent model peptide Suc-LY-AMC, and excess peptide was dialyzed out. At time $t = 0$, either active ClpP (red line) or inactive ClpP (black line) was added, and the fluorescence profile was recorded. At time $t = 120$ s, DTT was added to the mixture, resulting in a release of the peptide from the cysteine-linked ClpP. The released peptide was readily cleaved by the added active form of ClpP, resulting in an increase of the fluorescence (red line). The added inactive ClpP cannot cleave the model peptide and, as a result, the fluorescence does not change (black line).

interconverting states (23) (Fig. 3*a*; see also Fig. 6*a*, which is published as supporting information on the PNAS web site). When both isoleucines are fitted individually, very similar exchange parameters are extracted, consistent with a common exchange process, as suggested by the similar temperature dependence of the corresponding peak intensities. A global fit yields an exchange rate of $k_{ex} = k_{F\to S} + k_{S\to F} = 60.8\ (7.0)\ s^{-1}$ and similar populations, $p_F = 0.58\ (0.03)$, $p_S = 0.42\ (0.03)$, at 0.5°C.

The exchange process can be quantified in an independent way by using methyl TROSY relaxation dispersion measurements (20) (Fig. 3*b*). Here, the effective line width ($R_{2,eff}/\pi$) of correlations is measured as a function of the applied field strength, ν_{CPMG}, and the dependence is sensitive to exchange rates, populations of interconverting states, and both ^1H and ^{13}C chemical shift differences between states that can be measured directly from spectra recorded at 0.5°C (Fig. 2*a*, WT). As observed for the longitudinal exchange experiments, exchange parameters extracted for individual residues are very similar, and $k_{ex} = 67.5\ (2.5)\ s^{-1}$, $p_F = p_S = 0.5\ (0.02)$ were obtained from a global fit of the dispersion data. The utility of methyl TROSY techniques to access dynamic information on very large protein complexes can be appreciated from the similar exchange values obtained by means of the two independent methods.

The temperature dependence of the exchange parameters has been obtained by measuring longitudinal exchange between 0.5°C and 7°C (Fig. 3*c*). At higher temperatures, exchange contributions to the line widths of the correlations for I149 and I151 prevent the quantification of peak intensities. Over this limited temperature range, a clear increase in exchange rates is observed without a significant shift in populations (Fig. 6). At temperatures >35°C, the resonances of both isoleucines reappear at chemical shifts that are average between states F and S. Although the absence of discrete states precludes analysis by means of longitudinal exchange, extraction of exchange parameters is possible using dispersion measurements and the knowledge of the chemical shift differences observed at low temperature. The dispersion profiles fit very well to an increased exchange rate predicted from the extrapolation of the low-temperature data and to populations close to 1:1 (Fig. 3*c Inset*). Using measured exchange rates from 0.5°C to 40°C and transition state theory, values for the activation enthalpy [$\Delta H^{\ddagger} = 13.1\ (0.6)$ kcal·mol^{-1}] and entropy [$\Delta S^{\ddagger} = -3.6\ (2.3)$ cal·mol^{-1}·K^{-1}] for the F,S interconversion were calculated. Interestingly, the $\Delta H^{\ddagger}$ value obtained is similar to that reported previously for a localized conformational rearrangement in a cavity mutant of T4 lysozyme

(25). Populations of states F and S are nearly equal over the temperature range studied, indicating that both ΔG and ΔH are small (Fig. 6*b*). The small ΔG value (<0.3 kcal/mol) for the transition is consistent with the observation that the A153P mutation in *S. pneumoniae* ClpP leads to a dramatic destabilization of the handle domain, illustrating the low stability of this region (13).

A Link Between Dynamics and Function. How might the observed dynamics in the equatorial regions of the ClpP barrel be related to function? Insight is provided from a series of experiments where a cysteine is introduced at position 153 in helix E (ClpP A153C; Fig. 1*d*). Cysteines from two ClpP subunits in opposite rings are very close in space (1) (Fig. 1*d*) and readily form a disulfide bond under nonreducing conditions (Fig. 4*a*), thereby restricting the observed motional freedom of the handle region. NMR analysis of the cysteine mutant in the reduced, nonlinked state at low temperature shows, as expected from spectra of WT ClpP, four resonances for the two isoleucines in the handle region. Unfortunately, in the linked state, correlations involving these isoleucines were not observed at low temperature. The absence of correlations may reflect changes in chemical shifts and kinetics upon disulphide bond formation that broaden the resonances beyond detection and does not *a priori* rule out a significant shift in populations of states. NMR and CD spectra, under reducing and oxidizing conditions, however, clearly show that there are no global structural changes resulting from the introduced cysteine (Fig. 7, which is published as supporting information on the PNAS web site).

Under reducing conditions, ClpP A153C is active in degrading the model substrate protein GFP-SsrA (26) and the fluorescent peptide Suc-LY-AMC (27), although at only ≈50% of the activity of WT ClpP (Fig. 8 *a* and *b*, which is published as supporting information on the PNAS web site). This finding is consistent with our observations that mutations in the handle region often have a drastic effect on ClpP activity, most likely due to small rearrangements of the active site, which is located close to the handle region (Fig. 1*d*). The I151L mutant (Fig. 2*a*), for example, showed no proteolytic activity, although the chemical shifts of I149 and the other isoleucines are indistinguishable from WT ClpP. Stringent requirements on the orientation of the helical region might prevent activity of the unassembled or incorrectly assembled ClpP, thereby avoiding exposure of active protease sites.

The oxidized, linked form of ClpP has no proteolytic activity in peptide degradation experiments (Fig. 8*a*), which is most likely due to a distorted active site (see below). Surprisingly, however, when Suc-LY-AMC was added to oxidized ClpP A153C, the peptide was found to comigrate with the protease when the mixture was applied on a size-exclusion column (Fig. 8*c*), indicating that Suc-LY-AMC, at 200-fold molar excess over ClpP, was able to readily enter the protease lumen during the incubation period (≈30 min) and was retained in the protease during size-exclusion chromatography (≈45 min). In contrast, neither the reduced form of ClpP A153C nor WT ClpP showed retention of peptide (Fig. 8*c*).

To decouple the chemistry of substrate cleavage from peptide product release, further experiments were carried out with inactive forms of ClpP in which the catalytic Ser-111 is replaced by Ala (S111A; Fig. 4*a*). As with the active form of the enzyme, Suc-LY-AMC was retained in the oxidized, linked ClpP S111A A153C to a much greater extent than in the reduced, unlinked complex (Fig. 4*b Top*). Similar results were obtained by using a charged FLAG peptide, DYKDDDDK (data not shown). When the ClpP fraction containing Suc-LY-AMC (Fig. 4*b*) was isolated from the first column (fraction 6) and passed a second time over the column, the substrate comigrated with the protease under oxidizing conditions but was released from ClpP when the protease was reduced (Fig. 4*b Middle*). Under oxidizing conditions, the peptide was retained in ClpP for >10 h.

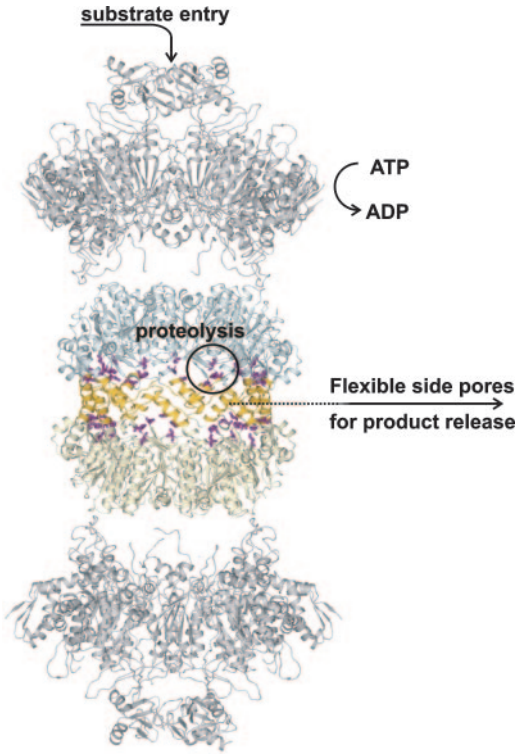

Fig. 5. Possible pathway of substrate entry and product release during degradation. The highly flexible helices are colored orange, and the active triad is shown in purple. A model of the ClpX chaperone (30) is shown on both sides of the ClpP barrel.

To ensure that the difference in peptide retention between cysteine-linked and reduced forms is not the result of the formation of a binding site for the peptide in the oxidized protease and to determine the role of the axial loops in retaining the peptide, control experiments were carried out using an N-terminal truncated version of ClpP S111A A153C (ClpP ΔN S111A A153C). As shown in Fig. 4*b Bottom*, this form of ClpP was unable to retain the peptide under either reducing or oxidizing conditions. Truncation of the N-terminal residues increases the size of the axial pores, allowing for an unobstructed passage of small peptides. Thus, this result indicates that a specific peptide-binding site is not formed within the ClpP proteolytic chamber upon oxidation of the cysteines and that the axial loops are important in mediating peptide retention. Moreover, the fact that ClpP ΔN A153C is unable to degrade substrates in the linked state but is active in the reduced form strongly suggests that the inactivity of the cysteine-linked form of ClpP is due to distortions of its active site and not its inability to release products.

The rapid release of substrate from the ClpP chamber upon reduction of the disulfide is further demonstrated in Fig. 4*c*. Here, active ClpP has been added to a sample of S111A A153C oxidized ClpP that was first incubated with fluorescent peptide and subsequently dialyzed to remove excess peptide, and the fluorescence profile has been measured (red curve). The peptide in the S111A A153C oxidized ClpP is clearly inaccessible to the active enzyme; however, upon addition of DTT, the peptide is readily released and is cleaved by the WT ClpP, leading to an increase in fluorescence (red curve). In the control experiment, where inactive ClpP (ClpP S111A) is added to ClpP S111A A153C with retained peptide, the baseline fluorescence level is maintained throughout the time course of the experiment; no cleavage of ligand occurs (black curve).

In conclusion, the present study demonstrates the use of NMR experiments to establish that the handle regions connecting the ClpP rings are highly dynamic and to characterize the kinetic and thermodynamic properties of the dynamic process. Biochemical approaches have been used, showing that cross-links between the E helices in the handle region significantly increase the retention time of peptide in the lumen of the enzyme relative to a reduced protein. Together, these results are consistent with the importance of dynamics in this region for the establishment of equatorial exit pores for the release of ClpP products. Exit of substrate through side pores provides a mechanism for the spatial separation of substrate entrance and product release when ClpX/A is bound to both axial pores simultaneously (Fig. 5), which may be an important component for the efficient and processive operation of the protease, allowing for continuous ClpX/A-mediated translocation of substrate into the proteolytic chamber through both axial pores at the same time (12, 28). The similarities in the structure and subunit arrangements between the members of cylindrical self-compartmentalizing proteases, and the fact that they all associate with ATPases that unfold and translocate substrates into an enclosed catalytic chamber for proteolysis (2, 3), suggest that the proposed model for peptide exit might be conserved. This work highlights the utility of methyl TROSY NMR spectroscopy to quantify site-specific dynamics in supramolecular structures and the power of a combined NMR-biochemistry approach for the study of biomolecular function.

We thank Prof. Julie Forman-Kay (Hospital for Sick Children, Toronto) for providing laboratory space for sample production and offering valuable comments; Dr. Ranjith Muhandiram for help with NMR; and Reagan Ching for making some of the ClpP mutants. This work was supported by grants from the Canadian Institutes of Health Research (to W.A.H. and L.E.K.) and a European Molecular Biology Organization postdoctoral fellowship (to R.S.). A.G. is a postdoctoral fellow of the Canadian Institutes for Health Research Strategic Training Program Grant in Protein Folding: Principles and Diseases. W.A.H. is a Canadian Institutes of Health Research New Investigator. L.E.K. is the recipient of a Canada Research Chair in Biochemistry.

1. Wang, J., Hartling, J. A. & Flanagan, J. M. (1997) *Cell* **91,** 447–456.
2. Wickner, S., Maurizi, M. R. & Gottesman, S. (1999) *Science* **286,** 1888–1893.
3. Pickart, C. M. & Cohen, R. E. (2004) *Nat. Rev. Mol. Cell Biol.* **5,** 177–187.
4. Bochtler, M., Ditzel, L., Groll, M. & Huber, R. (1997) *Proc. Natl. Acad. Sci. USA* **94,** 6070–6074.
5. Lowe, J., Stock, D., Jap, B., Zwickl, P., Baumeister, W. & Huber, R. (1995) *Science* **268,** 533–539.
6. Groll, M., Ditzel, L., Lowe, J., Stock, D., Bochtler, M., Bartunik, H. D. & Huber, R. (1997) *Nature* **386,** 463–471.
7. Ortega, J., Singh, S. K., Ishikawa, T., Maurizi, M. R. & Steven, A. C. (2000) *Mol. Cell* **6,** 1515–1521.
8. Sauer, R. T., Bolon, D. N., Burton, B. M., Burton, R. E., Flynn, J. M., Grant, R. A., Hersch, G. L., Joshi, S. A., Kenniston, J. A., Levchenko, I., *et al.* (2004) *Cell* **119,** 9–18.
9. Thompson, M. W., Singh, S. K. & Maurizi, M. R. (1994) *J. Biol. Chem.* **269,** 18209–18215.
10. Kim, Y. I., Burton, R. E., Burton, B. M., Sauer, R. T. & Baker, T. A. (2000) *Mol. Cell* **5,** 639–648.
11. Babbitt, S. E., Kiss, A., Deffenbaugh, A. E., Chang, Y. H., Bailly, E., Erdjument-Bromage, H., Tempst, P., Buranda, T., Sklar, L. A., Baumler, J., *et al.* (2005) *Cell* **121,** 553–565.
12. Ortega, J., Lee, H. S., Maurizi, M. R. & Steven, A. C. (2004) *J. Struct. Biol.* **146,** 217–226.
13. Gribun, A., Kimber, M. S., Ching, R., Sprangers, R., Fiebig, K. M. & Houry, W. A. (2005) *J. Biol. Chem.* **280,** 16158–16196.
14. Tugarinov, V., Hwang, P. M., Ollerenshaw, J. E. & Kay, L. E. (2003) *J. Am. Chem. Soc.* **125,** 10420–10428.
15. Tugarinov, V., Hwang, P. M. & Kay, L. E. (2004) *Annu. Rev. Biochem.* **73,** 107–146.
16. Goto, N. K., Gardner, K. H., Mueller, G. A., Willis, R. C. & Kay, L. E. (1999) *J. Biomol. NMR* **13,** 369–374.
17. Flanagan, J. M., Wall, J. S., Capel, M. S., Schneider, D. K. & Shanklin, J. (1995) *Biochemistry* **34,** 10910–10917.
18. Gardner, K. H. & Kay, L. E. (1997) *J. Am. Chem. Soc.* **119,** 7599–7600.
19. Delaglio, F., Grzesiek, S., Vuister, G. W., Zhu, G., Pfeifer, J. & Bax, A. (1995) *J. Biomol. NMR* **6,** 277–293.
20. Korzhnev, D. M., Kloiber, K., Kanelis, V., Tugarinov, V. & Kay, L. E. (2004) *J. Am. Chem. Soc.* **126,** 3964–3973.
21. Fiaux, J., Bertelsen, E. B., Horwich, A. L. & Wuthrich, K. (2002) *Nature* **418,** 207–211.
22. Pervushin, K., Riek, R., Wider, G. & Wuthrich, K. (1997) *Proc. Natl. Acad. Sci. USA* **94,** 12366–12371.
23. Farrow, N. A., Zhang, O., Forman-Kay, J. D. & Kay, L. E. (1994) *J. Biomol. NMR* **4,** 727–734.
24. Montelione, G. T. & Wagner, G. (1989) *J. Am. Chem. Soc.* **111,** 3096–3098.
25. Mulder, F. A., Mittermaier, A., Hon, B., Dahlquist, F. W. & Kay, L. E. (2001) *Nat. Struct. Biol.* **8,** 932–935.
26. Weber-Ban, E. U., Reid, B. G., Miranker, A. D. & Horwich, A. L. (1999) *Nature* **401,** 90–93.
27. Thompson, M. W. & Maurizi, M. R. (1994) *J. Biol. Chem.* **269,** 18201–18208.
28. Singh, S. K., Guo, F. & Maurizi, M. R. (1999) *Biochemistry* **38,** 14906–14915.
29. Kang, S. G., Maurizi, M. R., Thompson, M., Mueser, T. & Ahvazi, B. (2004) *J. Struct. Biol.* **148,** 338–352.
30. Kim, D. Y. & Kim, K. K. (2003) *J. Biol. Chem.* **278,** 50664–50670.